

System Identification and Signal Processing for PID Control of B0 Shim Systems in Ultra-High Field Magnetic Resonance Applications

Yu-Chun Chang* Nikolai Avdievich** Anke Henning***

*Max Planck Institute for Biological Cybernetics, Tübingen, Germany.
Graduate School of Neural & Behavioural Sciences, University of Tübingen, Tübingen, Germany
(e-mail: paul.chang@tuebingen.mpg.de).

**Max Planck Institute for Biological Cybernetics, Tübingen, Germany. (e-mail: nikolai.avdievitch@tuebingen.mpg.de)

***Max Planck Institute for Biological Cybernetics, Tübingen, Germany
Institute for Biomedical Engineering, University and ETH Zurich, Switzerland (e-mail: anke.henning@tuebingen.mpg.de)

Abstract: Magnetic resonance (MR) scanners are important tools in medical diagnostics and in many areas of neuroscience. MR technology is moving towards ultra-high field (UHF) 7T and 9.4T scanners which provide more signal intensity. However they also suffer from inhomogeneity of the static (B0) magnetic field which can lead to artifacts and uninterpretable data. B0 shimming is a technique used to reduce inhomogeneities but most MR scanners use static shim settings for the duration of the experiment. Dynamic shim updating (DSU) updates the shim in real-time while the scan is in process and can hence reduce any fluctuations in B0 field which may arise due to patient breathing, mechanical vibrations and so forth. However DSU is currently very slow and if we intend to increase the update rate then control theory needs to be applied. This paper presents an application of basic system identification and signal processing in the context of MR systems for DSU. Although system identification of these systems has been done before, they are non-parametric frequency domain approaches. These systems can be modelled as linear multivariable systems.

Keywords: Medical systems; gyromagnetic ratios; process identification; parameter optimization; smoothing filters; phase-locked loop; Hurwitz criterion; PID controllers.

1. INTRODUCTION

Magnetic resonance (MR) scanners are widely used in both clinical and research environments with a large range of applications, from medical diagnosis to research in psychological neuroscience. In MR imaging (MRI), higher magnetic field strength of the static magnetic field (referred to as the B0 field) results in higher signal intensity and therefore a higher spatial resolution and a decrease in scan time (Takahashi, 2003). This is particularly beneficial in functional MRI where time resolution is important. Furthermore in MR spectroscopy (MRS), higher fields result in higher frequency separation between spectral resonances and also allow the detection of smaller concentrations of metabolites (Xu and Vigneron 2011). These benefits have led to the development of higher magnetic fields from 1.5T and 3T scanners to ultra-high field (UHF) 7T and 9.4T scanners.

Naturally, certain disadvantages also come with the benefits of high fields. UHF systems have higher specific absorption rates (SAR) which relates to how much RF energy is absorbed by the patient. The homogeneity of the static B0 field is also an issue at all field strengths but especially at UHF and is particularly important in MR spectroscopy (De Graaf, 2003). There are many more advantages and disadvantages of UHF but only the problem of B0 inhomogeneity shall be discussed in this paper.

1.1 B0 Shimming

Shimming is the processes of adjusting the static magnetic field to make it more homogeneous. There are two types of shimming: passive and active (De Graaf, 2007). Passive shimming uses pieces of ferromagnetic material to optimise the homogeneity. Once this optimisation has been done, it cannot be changed. Active shimming uses coils to generate the optimum magnetic field adjustments by driving them with the appropriate current.

Active shimming can be either static or dynamic. For static shimming, the optimal adjustments are made before the scan and remain the same for the duration of the scan. Most MR systems that have shimming functionality use static shimming. On the other hand, dynamic shimming automatically updates the shim during the scan. Dynamic shim updating (DSU) is a field of study that has only recently attracted the attention of the MR community.

DSU has been used to correct for fluctuations in the field due to breathing (see Boer et al., 2012 and Wilm et al., 2013). Since breathing is relatively slow, the shim update rate is slow and also much slower than the shim system. The feedback loops typically use digital proportional-integrator (PI) controllers (Wilm et al., 2013). Furthermore stability is not an issue because the open-loop system is stable and settles in less than

one time sample thus the PI controller does not have to be designed based on the open-loop system.

Certain applications would benefit from a high time resolution closed-loop control of the shim system. For example, dynamically updating the shim settings for every slice or volume of interest during an image acquisition sequence (Koch et al., 2006; Juchem et al., 2010) and updating shim settings for a moving volume of interest (Schär et al., 2004). These fast switching currents generate eddy currents which need to be compensated for. Thus if the system is to be controlled at a much smaller time scale such that the update rate is faster than the open-loop system then controllers based on the open-loop system need to be designed. Controller design based on a system model with a fast update rate is proposed in this paper.

1.2 System Identification of Shim Systems

To identify the system we need to measure the response of the static magnetic field. Jezzard and Balaban (1995) show that the B_0 field can be determined from phase maps. However, obtaining phase maps is too slow and cannot capture the dynamics of the system. A more effective method for measuring the B_0 field is to use nuclear MR (NMR) field probes (Barnet et al., 2008; and Handwerker et al., 2013).

1.3 Outline

Section 2 describes the hardware that was available and the process of manufacturing the sensors and instrumentation. This section also includes the signal processing methods that were used and proposes a hybrid filter for reducing noisy measurements. Section 3 presents the method used for system identification. An example of how PID controllers can be designed is shown in section 4 and their simulated results also included. Finally section 5 draws the conclusions and makes further recommendations for improving B_0 shimming.

2. INSTRUMENTATION AND SIGNAL PROCESSING

2.1 Hardware and Sensors

The experiments were performed on a whole-body 9.4T Siemens Magnetom MR scanner (Erlangen, Germany).

A custom built 9.4T field camera consisting of sixteen 1H field probes was used to monitor the field (fig. 1). De Zanche et al. (2008) describes the process for producing NMR probes. The probes were constructed using water samples doped with CuSO_4 at a ratio of 3.7g/l to decrease the T_1 relaxation time to approximately 80ms. Each coils consisted of six turns around a 1.0mm outer diameter and 0.8mm inner diameter glass tube where the tube was a length on 10mm. Each probe was encapsulated in epoxy and doped with $\text{Dy(III)(NO}_3)_3 \cdot 5\text{H}_2\text{O}$ at a ratio of 2.75mg per 5g of epoxy for susceptibility matching to the copper wire. The probes were arranged on a spherical mount with a diameter of 250mm.

Each of the probes were tuned to the appropriate frequency of 399.72MHz (given by $\omega = \gamma \times B_0$ where γ is the gyromagnetic ratio). The probes were matched to 50Ω and decoupled using cable traps with an isolation of more than 42dB between any

two probes. The probes were operated in transmit/receive mode using a custom-build 16 channel interface (-50dB isolation, 0.2dB insertion loss per channel). A rectangular RF excitation pulse of 0.5ms duration was used and the signals were sampled at 300kHz.

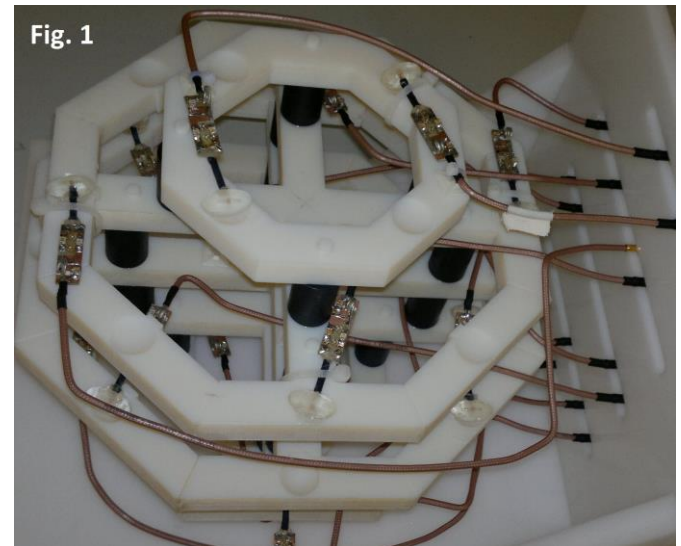


Fig. 1. Magnetic field camera with 16 NMR probes for spatio-temporal monitoring of the B_0 field.

2.2 Input and Output Signals

The input signals to the system were the current signals used to drive the shim coils. The output of the system is the B_0 field, which can be described using a set of basis functions as

$$|\mathbf{B}(\mathbf{r}, t)| = \sum_{i=0}^{N_L-1} c_i(t) f_i(\mathbf{r}) + B_{ref}(\mathbf{r})$$

where \mathbf{r} is the position in space, $f_i(\mathbf{r})$ is the set of basis functions, $c_i(t)$ are the field coefficients, N_L is the number of basis functions and $B_{ref}(\mathbf{r})$ is the reference field some initial time t_0 (see Barnet et al., 2008). Spherical harmonic (SH) functions are used as the basis functions because the shim coils are designed to generate the SH components of the field (Clare et al., 2006). Molecules subject to a magnetic field $\mathbf{B}(\mathbf{r}, t)$ and a gyromagnetic ratio γ accrue a phase given by $\varphi(t) = \gamma \int_0^t B(t') dt'$. Therefore the field coefficients that characterise the B_0 field are related to the phase coefficients by

$$c_i(t) = \frac{1}{\gamma} \cdot \frac{dk_i(t)}{dt} \quad i = 0, \dots, N_L - 1$$

where $k_i(t)$ are given by fitting basis functions to the phase maps (Vannesjo et al., 2013).

The NMR probes measure the free-induction decay (FID) of the molecules (Handwerker, 2013). The FID phase of a probe at position \mathbf{r} is the phase $\varphi(\mathbf{r}, t)$. The field coefficients $c_i(t)$ can then be calculated using SH basis functions as described by Barnet et al. (2008).

2.3 Hybrid Filter

The probes are small for high spatial resolution and specificity but this results in noisy FIDs. Furthermore since the field

coefficients are dependent on the derivative of the phase signals, phase jitter makes the field measurements noisier.

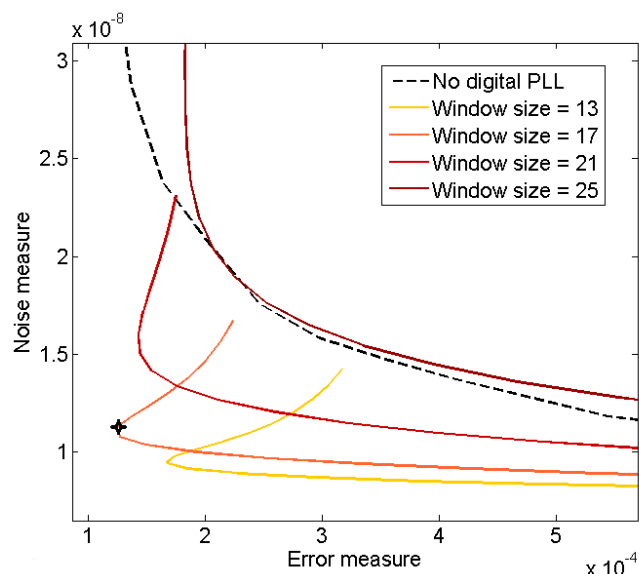


Fig. 2. Comparison of the digital PLL with a moving-average filter. PLL filters with bandwidths ranging from 200 to 800 times greater than the bandwidth of the gradient system. The performance of a moving-average is shown as a reference (window sizes from 3 to 41 samples).

Phase locked-loop (PLL) filters can be used to reduce phase jitter. A second-order digital PLL was used and the closed-loop transfer function in the z-domain is

$$H(z) = \frac{\gamma((1 + \rho)z - 1)}{z^2 + (\gamma + \gamma\rho - 2)z + (1 - \gamma)}$$

where γ and ρ are the design parameters (Shayan and Le-Ngoc, 1989). The filter poles were constrained to be real and equal.

The input signal was a gradient in the x-direction switched on and off to produce a triangular wave-form. The gradient amplitude was 5mT/m and the slew rate was 40mT/m/ms.

Two objectives were considered when filtering: minimizing noise and preserving the underlying signal (i.e. avoid over-smoothing). A moving-average filter was able to outperform the PLL in both objectives. The noise measure is the square sum of the error signal when the output signal is in steady-state. The preservation measure is the square sum of the difference between the filtered signal and the predicted response. The predicted response was found using a basic system identification method (as described in section 3).

A hybrid filter using the PLL and moving-average filters was investigated. A range of moving-average window sizes, varying from 3 to 41 samples, was used. The closed-loop response of the PLL needs to be much faster than the system. A range of PLL filters were tested where γ was 200 to 800 times faster than the system response time. Fig. 2 shows the performance of the different combinations of γ and the window size. Hence we can find optimal parameters for reduce noise and preserve the actual signal. The cross in fig. 2 was chosen as the optimal point its performance is shown in fig. 3. Fig. 3

shows a comparison of the time domain signals for the PLL filter, moving-average, and the hybrid filter.

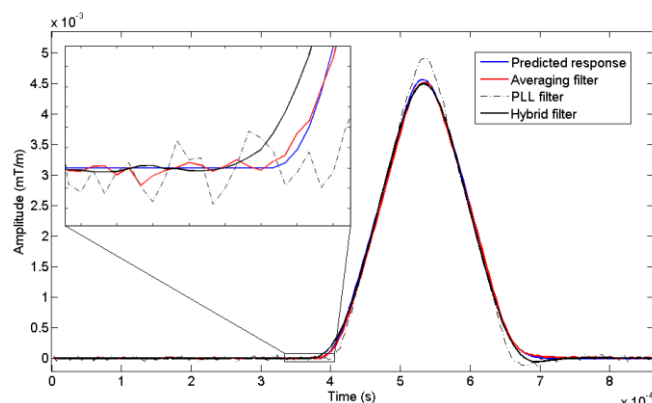


Fig.3. Time domain plots of the derivatives of the phase signals after being processed with different filters. The moving-average filter window size is 13. The PLL filter bandwidth is 360 times greater than the gradient system. The hybrid filter is the same as the PLL but with a moving-average with window size 17 (optimal point as shown in fig. 2).

3. SYSTEM IDENTIFICATION

Until this point, shim systems have been exclusively mentioned. However, notice that the gradient system are the set of linear shim terms. The integrated shim system of the scanner could not be changed during an experiment and therefore only gradient coils were used and so there are three inputs: x-, y- and z-gradients. The output signals were the field coefficients. The zero to second-order SH functions can be calculated from the 16 probes which gives a total of nine output functions.

Each transfer function is assumed to be at most a second-order system and with no dead-time, so the transfer functions in the s-domain are:

$$g(s) = \frac{A\omega}{s^2 + 2as + (a^2 + \omega^2)} \text{ or } g(s) = \frac{A}{s+a}$$

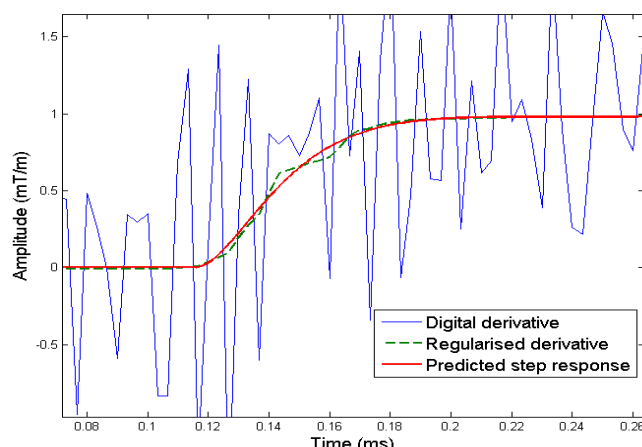


Fig. 4. Derivative of the field coefficient during the gradient ramp period of the x-gradient (slew rate 43.5mT/m/ms). The gradient was started at 0.12ms. The digital finite difference derivative.

Due to hardware limitations, step inputs could not be applied to obtain the step responses. Instead, ramp inputs were used

and the derivative of the output signal gave the step response. To calculate the derivative of the output signals (to find the step response from the ramp response), the finite difference derivative was found to be too noisy. Therefore a total regularisation derivative method proposed by Chartrand (2011) was used to calculate a smooth derivative. The difference between the digital derivative and the regularised derivative is shown in fig. 4. A regularisation factor of $\alpha = 5e^{-6}$ was used.

Table I: System model

Input	Output	A	a	ω
Gx	F0	5.23e3	31.4e3	-
Gx	X	133.3e3	54.4e3	27.2e3
Gx	XY	-1.99e3	33.4e3	-
Gx	Z2	-2.67e3	36.6e3	-
Gx	X2+Y2	4.06e3	0	34.5e3
Gy	F0	-1.78	27.8e3	-
Gy	Y	86.98e3	42.8e3	35.8e3
Gy	XY	3.95e3	29.2e3	-
Gz	Z	86.31e3	42.4e3	34.2e3
Gz	YZ	-0.737e3	19.4e3	-
Gz	XZ	3.21e3	28.4e3	-

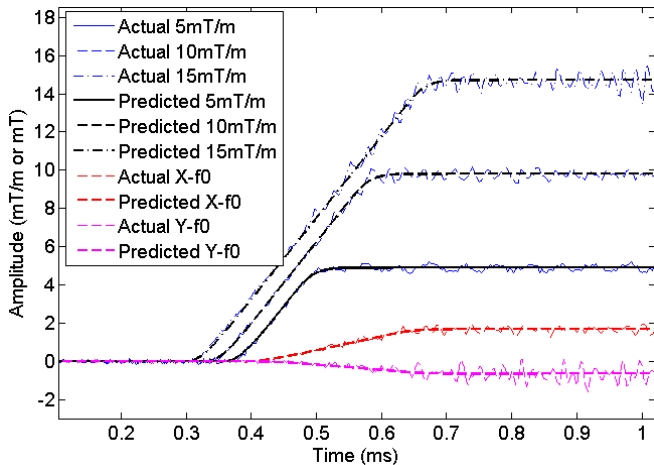


Fig. 5. Predicted and actual response of the x-gradient for different amplitudes. The cross-terms of the x- and y- gradients (10mT/m) to the zero-order term (mT) are also shown.

Using the derivative as the step response, the transfer function could be fit to the data. The slew rate was set to 43.5mT/m/ms and this corresponds to the amplitude of the step input. The system model was fit to the data and the optimal values (in the least-squares sense) for the parameters A , a and ω were found. The step response of the fitted transfer function is shown in fig. 4. The complete system is given in table I; transfer functions where the ω is omitted refer to first-order systems.

To verify the results, the predicted output from the applied input (10mT/m with 43.5mT/m/ms slew rate) was compared to the actual output. This was also done for gradient input amplitudes of 5mT/m and 15mT/m for each of the gradient inputs. Fig. 5 shows the time domain responses of the x-gradient input.

4. CLOSED-LOOP SIMULATION

4.1 PID Controller Design

Only the first-order shim coils (input) – called the gradient coils – and first-order SH terms (output) were considered. This results in three independent single-input single-output (SISO) systems which is unsurprising as the gradients are coils are decoupled and shielded from each other.

The gradient system is controlled with an inner closed-loop circuit that controls the current. Our goal is to control the slower outer loop to make it robust against noise and disturbances and not necessarily improve the speed of the system. The setpoint signal for the inner current control loop is a digital signal and hence the aim is to design digital controllers for the outer loop. PID controllers were designed for each of the three systems to test for feasibility of the digital controllers. PID controllers are well-known and the transfer function can be defined as

$$K_{PID}(s) = K_p + K_I/s + K_D s / (1 + T_F s)$$

where the design parameters are $\theta = [K_p, K_I, K_D, T_F]$. The PID controllers were designed using a multi-objective optimisation approach. The optimal points are defined using the Pareto dominance condition. Suppose there are two fitness functions $F(\theta) = [F_1(\theta), F_2(\theta)]$ where θ is the domain variable (in this case, the design parameter vector), then θ_1 Pareto dominates θ_2 if

$$[F_1(\theta_1) < F_1(\theta_2) \text{ and } F_2(\theta_1) \leq F_2(\theta_2)] \text{ or}$$

$$[F_1(\theta_1) \leq F_1(\theta_2) \text{ and } F_2(\theta_1) < F_2(\theta_2)]$$

where we suppose that we want to minimise F . This can be extended to more fitness functions. A formal description of Pareto optimality is given in Hajiloo et al. (2008).

Firstly the fitness functions need to be defined. Hajiloo et al. (2008) use Pareto optimum design to find a set of robust PI and PID controllers. Popov et al. (2005) analyse the trade-off between the controller performance (integral squared error) and the controller effort, while Sabahi et al. (2008) consider the trade-off between performance (settling time) and the robustness (over/undershoot). Considering these previous fitness functions, three objectives were chosen: the performance, the robustness and the control effort. The performance was measured using the settling time, the control effort was measured using the infinity-norm on the control signal and the robustness was measured using the infinity norm of the sensitivity and complementary sensitivity (Garcia et al., 2007). These fitness functions were to be minimised

1. Settling time: $\left| \frac{y_\infty - y(t)}{y_\infty} \right| < 0.05 \quad t > t_0$
2. Sensitivity: $\left\| \frac{1}{1+gk} \right\|_\infty$

3. Complementary sensitivity: $\left\| \frac{gk}{1+gk} \right\|_{\infty}$
4. Control effort: $\left\| \frac{k}{1+gk} \right\|_{\infty}$

Given that the plant and controller are both second-order system, the closed-loop system is fourth -order and the characteristic equation is given by

$$\begin{aligned} \varphi(s) &= T_F \cdot s^4 + (1 + 2aT_F)s^3 \\ &+ (2a + T_F(a^2 + \omega^2) + T_F K_P A \omega)s^2 \\ &+ ((a^2 + \omega^2) + (K_P + T_F K_I + K_D)A \omega)s + K_I A \omega \end{aligned}$$

Constraints for the parameters were then obtained from the Hurwitz stability criteria. The domain space for θ was defined by considering the Routh-Hurwitz stability criteria and by requiring firstly, that the closed-loop system cannot be much slower than the open-loop system (settling time with 20% of the open-loop), and secondly, requiring the noise to be sufficiently reduced the filter time constant T_F was chosen to be between $1e-5$ and $1e-3$ and lastly, requiring the K_P cannot exceed some upper bound (chosen as 1.0).

Table II. Chosen Optimal PID Controller Parameters

	K_P	K_I	K_D	T_F
x-Grad	0.051	14.06e3	-0.197	20e-5
y-Grad	0.213	19.10e3	-0.073	2.11e-5
z-Grad	0.538	23.51e3	-0.243	2.23e-5

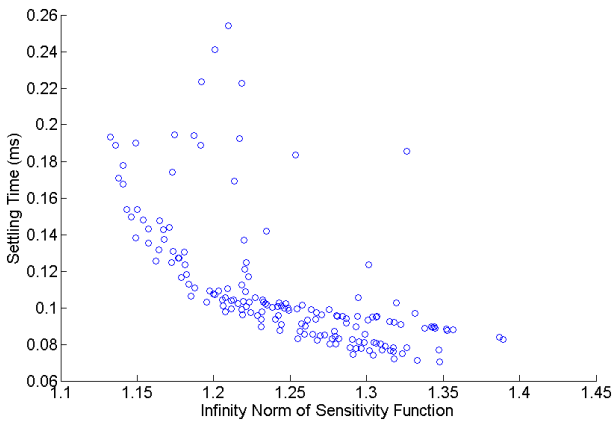


Fig. 6. Trade-off between the closed-loop performance (measured with the settling time) and robustness (measured with the sensitivity function) of PID controllers for the z-gradient system.

Since the domain space was defined to be relatively small, a brute-force search method was used to find the Pareto-optimal points. The infinity-norm complementary sensitivity of the Pareto-optimal points were found to be very similar (close to 1.0) thus providing little additional information and so was discarded as a fitness function. This left three fitness functions which was easier to visualise. The trade-off between the sensitivity and settling time (for the z-gradient system) is shown in fig. 6. The optimum point was chosen to be the minimum sensitivity where the closed-loop and open-loop settling times are equal. The corresponding PID parameters θ

can then be found from this point. The PID controllers for the x-, y- and z-gradients were all designed in this manner. The chosen PID parameters are shown in table II.

4.2 Closed-Loop Simulation

The closed-loop systems of each gradient was simulated to verify the results of the PID controllers. These simulations were also used to obtain hardware specifications for implementation of these controllers digitally.

The time domain simulations show that the systems have good disturbance rejection and low sensitivity to noise. Fig. 7 shows these results for the z-gradient however the x- and y-systems were very similar. Furthermore, the figure shows that the closed-loop system is as fast as the open-loop system (as given by the design criteria). The analogue PID controllers were converted to digital controllers using a bilinear transformation (Tustin's method) without pre-warping (see Al-Alaoui, 2007). The sampling rate shown in fig. 7 is 20kHz. As the sampling rate decreases, the system starts to oscillate more until the sampling rate is so low that the system becomes unstable. Therefore for digital controller implementation it is recommended that the sampling rate (or rather update rate) is at least 20kHz. For fast and effective closed-loop control of the gradient system with a digital controller, an embedded system is recommended rather than a microcontroller since most off-the-shelf microcontrollers are generally not fast enough.

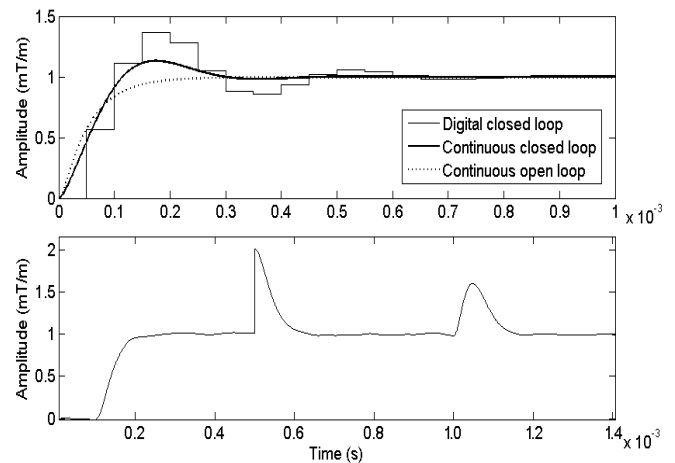


Fig. 7. Time domain simulation of the continuous open-loop plant, the continuous closed-loop system and the digital closed-loop system for the z-gradient system (top). Time domain plot of the continuous closed-loop system for the z-gradient with a step input at $t=0.1$ ms, an output disturbance (1mT/m) at $t=0.5$ ms and an input disturbance (1mT/m) at $t=1.0$ ms and white measurement noise from -2 to 2mT/m (bottom).

5. CONCLUSION

A field camera consisting of 16 NMR probes was built to measure the B0 magnetic field. Filters for processing the phase signals measured by the probes were investigated and a hybrid filter utilising a moving average and a phase locked-loop filter was proposed. System identification was performed on a 9.4T MR gradient system using standard first- and second-order parametric models. PID controllers were designed for the system and the closed-loop responses were simulated.

With the current field camera, the system model can be easily extended to identify a multivariable shim system of up to second-order SH. Unlike the linear SH terms where the systems are independent, gradients also affect higher order terms (see also Vannesjo et al., 2013). Juchem et al. (2010) also show that higher order shim coils can affect other SH terms. Therefore controller design for shim systems require multivariable control techniques.

Analogue PID controllers were designed and the results were simulated. The analogue controllers were used to evaluate the required update rate for implementation of digital controllers. It is recommended that the update rate needs to be at least 20kHz to ensure stability.

ACKNOWLEDGEMENTS

The authors would like to thank Martin Eschelbach at the Max Planck Institute for Biological Cybernetics for his contributions on providing information about the process for the manufacturing of the NMR probes.

REFERENCES

- Al-Alaoui, M.A. (2007). Novel approach to analog-to-digital transforms. *IEEE Transactions on Circuits and Systems-I: Regular Papers*, 54(2), 338-350.
- Barnet, C., De Zanche, N., and Pruessmann, K.P. (2008). Spatiotemporal magnetic field monitoring for MR. *Magnetic Resonance in Medicine*, 60, 187-197.
- Boer, V.O., van Vliet, G., Luijten P.R., and Klomp D.W. (2012). Direct B0 field monitoring and real-time B0 field updating in the human breast. *Magnetic Resonance in Medicine*, 67, 586-591.
- Chartrand, R. (2011). Numerical differentiation of noisy, non-smooth data. *ISRN Applied Mathematics*, 2011.
- Clare, S., Evans, J., and Jezzard, P. (2006). Requirements for room temperature shimming of the human brain. *Magnetic Resonance in Medicine*, 55, 210-214.
- De Graaf, R.A., Brown, P.B., McIntyre, S., Rothman, D.L. (2003). Dynamic shim updating (DSU) for multislice signal acquisition. *Magnetic Resonance in Medicine*, 49, 409-416.
- De Graaf, R.A. (2007). *In Vivo NMR Spectroscopy: Principles and Techniques (2nd ed.)*, ch. 10: Hardware. John Wiley&Sons Ltd. England.
- De Zanche, N., Barnet, C., Nordmeyer-Massner, J.A., and Pruessman, K.P. (2008). NMR probes for measuring magnetic fields and field dynamics in MR systems. *Magnetic Resonance in Medicine*, 60, 176-186.
- Garcia, D., Karimi, A., and Longchamp, R. (2007). Robust proportional integral derivative controller tuning with specifications on the infinity-norm of sensitivity functions. *IET Control Theory Applications*, 1(1), 263-272.
- Hajiloo, A., Nariman-zadeh, N., and Moeini, A. (2008). Pareto optimum design of robust controllers for systems with parametric uncertainties. P. Pecherkova, M Flidr and J Dunik (ed.), *Robotics, Automation and Control*, ch. 12, 205-226. Vienna, Austria.
- Handwerker, J., Ortmanns, M., Anders, J., Eschelbach, M., Chang, P., and Scheffler, K. (2013). An active TX/RX NMR probe for real-time monitoring of MRI field imperfections. *Proceedings of IEEE Biomedical Circuits and Systems Conference*. Netherlands, Oct 2013.
- Jezzard, P., and Balaban, R.S. (1995). Correction for geometric distortion in echo planar images from B0 field variations. *Magnetic Resonance in Medicine*, 34 (1), 65-73.
- Juchem, C., Nixon, T.W., Diduch, P., Rothman, D.L., Starewicz, P., and de Graaf, R.A. (2010). Dynamic shimming of the human brain at 7T. *Concepts in Magnetic Resonance B*, 37(3), 116-128.
- Koch, K.M., McIntyre, S., Nixon, T.W., Rothman, D.L., and de Graaf, R.A. (2006). Dynamic shim updating on the human brain. *Journal of Magnetic Resonance*, 180, 286-296.
- Popov, A., Farag, A., and Werner, H. (2005). Tuning of a PID controller using a multi-objective optimization technique applied to a neutralization plant. *Proc. of the 44th IEEE Conference on Decision and Control*. Spain, Dec 2005.
- Sabahi, K., Sharifi, A., Aliyari Sh., M., Teshnehlab, M., and Aliasghary, M. (2008). Load frequency control in interconnected power system using multi-objective PID controller. *Journal of Applied Sciences*, 8(20), 3676-3682.
- Schär, M., Kozerke, S., and Boesiger, P. (2004) Navigator gating and volume tracking for double-triggered cardiac proton spectroscopy at 3 Tesla. *Magnetic Resonance in Medicine*, 51, 1091-1095.
- Shayan, Y.R., and Le-Ngoc, T. (1989). All digital phase-locked loop: concepts, design and applications. *IEE Proceedings F*, 136(1), 53-56, Feb 1989.
- Takahashi, M., Uematsu H., and Hatabu, H. (2003). MR imaging at high magnetic fields. *European Journal of Radiology*, 46, 45-52.
- Vannesjo, S.J., Haeberlin, M., Kasper, L., Pavan, M., Wilm, B.J., Barnet, C., and Pruessman, K.P. (2013). Gradient system characterization by impulse response measurements with a dynamic field camera. *Magnetic Resonance in Medicine*, 69, 583-593.
- Wilm, B.J., Duerst Y., Dietrich B.E., Wyss, M., Vannesjo, S.J., Schmid, T., Brunner, D.O., Barnet, C., and Pruessmann, K.P. (2013). Feedback field control improves linewidths in *in vivo* magnetic resonance spectroscopy. *Magnetic Resonance in Medicine*, doi: 10.1002/mrm.24836.
- Xu, D., and Vigneron, D.B. (2011). High field MR spectroscopy: Investigating human metabolite levels at high spectral and spatial resolution. J. Hennig and O. Speck (ed.), *High-Field MR Imaging*, 215-228. Springer, Berlin Heidelberg.